

1           **RIP1-HAT1-SirT complex identification and targeting in treatment and prevention of cancer**

2  
3   Vincenzo Carafa<sup>1</sup>, Angela Nebbioso<sup>1</sup>, Francesca Cuomo<sup>1</sup>, Dante Rotili<sup>2</sup>, Gilda Cobellis<sup>1</sup>, Paola Bontempo<sup>1</sup>,  
4   Alfonso Baldi<sup>3</sup>, Enrico P. Spugnini<sup>4</sup>, Gennaro Citro<sup>5</sup>, Angela Chambery<sup>3</sup>, Rosita Russo<sup>3</sup>, Menotti Ruvo<sup>6</sup>,  
5   Paolo Ciana<sup>7</sup>, Luca Maravigna<sup>7</sup>, Jani Shaik<sup>8</sup>, Enrico Radaelli<sup>9,10</sup>, Pasquale De Antonellis<sup>11</sup>, Domenico  
6   Tarantino<sup>2</sup>, Adele Pirolli<sup>2</sup>, Rino Ragno<sup>2</sup>, Massimo Zollo<sup>11,12</sup>, Hendrik G. Stunnenberg<sup>8</sup>, Antonello Mai<sup>2,13</sup>,  
7   Lucia Altucci<sup>1\*</sup>

8  
9   <sup>1</sup> Dipartimento di Medicina di Precisione, Università della Campania Luigi Vanvitelli, Napoli, IT; <sup>2</sup>  
10   Dipartimento di Chimica e Tecnologie del Farmaco "Sapienza" Università di Roma, 00185 Roma, IT; <sup>3</sup>  
11   Dipartimento di Scienze e Tecnologie Ambientali Biologiche e Farmaceutiche Università della Campania  
12   Luigi Vanvitelli, CE, IT; <sup>4</sup> Biopulse s.r.l., Napoli, IT; <sup>5</sup> SAFU Department, Regina Elena Cancer Institute; <sup>6</sup>  
13   Istituto di Biostrutture e Bioimmagini, CNR, and CIRPeB, 80134, Napoli, IT; <sup>7</sup> Center of Excellence on  
14   Neurodegenerative Diseases and Department of Pharmacological Sciences, Università di Milano, IT; <sup>8</sup>  
15   Department of Molecular Biology, Radboud University, 6500 HB Nijmegen, NL; <sup>9</sup> Mouse & Animal  
16   Pathology Lab, Fondazione Filarete, 20139, Milano, IT; <sup>10</sup> University of Pennsylvania, School of Veterinary  
17   Medicine, Department of Pathobiology Philadelphia, PA 19104-6051, United States; <sup>11</sup> CEINGE 80145  
18   Naples, IT; <sup>12</sup> Dipartimento di Biochimica e Biotecnologie Mediche, Università Federico II 80145 NA, IT; <sup>13</sup>  
19   Pasteur-Fondazione Cenci Bolognetti, Sapienza Università di Roma, 00185 Roma, Italy.

20  
21   \* **Corrispondence:** Prof. Lucia Altucci: Università degli Studi della Campania Luigi Vanvitelli,  
22   Dipartimento di Biochimica Biofisica e Patologia Generale, Vico De Crecchio 7, 80138 Napoli, IT; Ph +39-  
23   0815667569; Fax +39-081450169; email: [lucia.altucci@unicampania.it](mailto:lucia.altucci@unicampania.it)

24  
25   **Running title:** RIP1-HAT1-SirT complex in cancer

26   **Key words:** Cancer, Epigenetics, Acetylation, Sirtuins, Apoptosis, Necroptosis.

27  
28   **Conflict of interest statement:** The authors declare that they have no conflicts of interest.

## 34 **Abstract**

35 **Purpose:** Alteration in cell death is a hallmark of cancer. A functional role regulating survival, apoptosis and  
36 necroptosis has been attributed to RIP1/3 complexes.

37 **Experimental design:** We have investigated the role of RIP1 and the effects of MC2494 in cell death  
38 induction, using different methods as flow cytometry, transcriptome analysis, immunoprecipitation,  
39 enzymatic assays, transfections, mutagenesis and *in vivo* studies with different mice models.

40 **Results:** Here, we show that RIP1 is highly expressed in cancer and we define a novel RIP1/3-SIRT1/2-  
41 HAT1/4 complex. Mass Spectrometry identified 5 acetylations in the kinase and death domain of RIP1. The  
42 novel characterised pan-SirT inhibitor, MC2494, increases RIP1 acetylation at 2 additional sites in the death  
43 domain. Mutagenesis of the acetylated lysine decreases RIP1-dependent cell death suggesting a role for  
44 acetylation of the RIP1 complex in cell death modulation. Accordingly, MC2494 displays tumour-selective  
45 potential *in vitro*, in leukemic blasts *ex vivo*, and *in vivo* in both xenograft and allograft cancer models.  
46 Mechanistically, MC2494 induces *bona fide* tumour-restricted acetylated RIP1/caspase-8-mediated  
47 apoptosis. Excitingly, MC2494 displays tumour-preventive activity by blocking DMBA-induced mammary  
48 gland hyper-proliferation *in vivo*.

49 **Conclusions:** These preventive features might prove useful in patients who may benefit from a recurrence-  
50 preventive approach with low toxicity during follow-up phases and in cases of established cancer  
51 predisposition. Thus, targeting the newly identified RIP1 complex may represent an attractive novel  
52 paradigm in cancer treatment and prevention.

53

## 54 **Translational Relevance**

55 It is becoming increasingly clear that cancer is not only a genetic but also an epigenetic disease. Here,  
56 we identified a novel RIP1-SirT/HAT1 complex controlling survival and death via regulation of RIP1  
57 acetylation. Notwithstanding the increasing interest for sirtuins modulation in tumorigenesis, very little  
58 known is on their involvement in programmed cell death programs. A major goal of epi-drug development is  
59 to increase the therapeutic index and limit development of resistance. One attractive option is to combine  
60 anticancer effects with drugs able to prevent neoplasia. Here, we have developed and report on a novel pan-  
61 SirT inhibitor that alters HAT1/SirT equilibrium in the RIP1 complex, showing *bona fide* anticancer-  
62 selective and cancer-preventive activities *in vitro*, *ex vivo* and *in vivo*. Our work expands the current views in  
63 the drug discovery and might prove useful in patients who may benefit from a recurrence-preventive  
64 approach with low toxicity during follow-up phases and in cases of established cancer predisposition.

65

66

67

68

69

70

## 71 **Introduction**

72 Cell death is a normal process responsible of tissue homeostasis. Different pathways of cell death have been  
73 described (1) and recently classified (2,3). Both the classical apoptosis, autophagy and necroptosis (a new  
74 form of programmed cell death) (4) have been causally connected to cancer. The RIP1 kinase has been  
75 reported displaying a functional role in either regulation of survival or apoptosis and necroptosis (5) and is a  
76 key regulator of many signalling pathways such as inflammation (6), oxidative stress, plasma membrane  
77 permeabilization and cytosolic ATP reduction (7). RIP1, initially identified as a Fas-interacting protein (8,9),  
78 is also named ‘a death domain kinase’, having a 112 amino acid death domain (DD) at its C-terminus. RIP1  
79 is the founding member of the RIP family (10). RIP1 kinase activity is responsible for RIP3 phosphorylation  
80 (11), and subsequently, for MLKL phosphorylation and trimerization, which is necessary to activate the  
81 necroptotic death pathway (12,13). The fact that other RIP family members do not compensate for RIP1-  
82 deficiency suggests a unique role for RIP1(10,14). The central deregulation of cell death in tumorigenesis  
83 has become clear, yet, very little is known of RIP1 and cancer. RIP1 and RIP3, as well as necroptosis, are  
84 deregulated in many types of cancers thus presenting a potential therapeutic targets in treatment of cancers  
85 resistant to chemotherapeutic agents or to apoptosis inducers (15,16). Here, we show that RIP1 is highly  
86 expressed in cancer and we define a novel RIP1/3-SIRT1/2-HAT1/4 complex in which RIP1 is subject to  
87 regulation by acetylation. Excitingly, mutation of the acetylated lysine decreases RIP1-dependent cell death,  
88 suggesting a role for acetylation of the RIP1 complex in cell death deregulation and function. Increasing  
89 RIP1 acetylation with a novel multi-acting SirT inhibitor, MC2494, displays tumor-selective therapeutic  
90 potential *in vitro*, *ex vivo*, and *in vivo* inducing tumour-restricted apoptosis. Extraordinarily, MC2494 shows  
91 tumour-preventive activity *in vivo*. Thus, targeting the newly identified RIP1 complex and its acetylation  
92 may represent a feasible and attractive novel paradigm for therapeutic purposes in cancer treatment and  
93 prevention.

94

## 95 **Materials and Methods**

96 **Cell lines, primary cells and ligands.** U937, NB4, HL-60, K562, U266, JURKAT, MCF7, MDA-MB231,  
97 LnCap, NIH3T3 and HCT116 cells, were purchased from DSMZ. MCF10A was purchased from ATCC.  
98 HEK293FT and HACAT cells, were ordered from Thermo Fisher Scientific. EPN, hMSC and Primary  
99 normal amniocytes cells, were obtained from University of Campania Luigi Vanvitelli, IT. All cell lines and  
100 primary cells were grown following standard protocols. A more detailed description is reported in  
101 Supplementary Material and Methods. Mycoplasma contamination was regularly examined using EZ-PCR  
102 Mycoplasma kit (Biological Industries), prior to freezing working stabs. All cell lines were tested and  
103 authenticated. Cells were used for experiments within 10-20 passages and then discarded. AGK2 (Sigma),  
104 MC2494 (and derivatives) were dissolved in DMSO and used at  $5 \times 10^{-5}$  M. MC2494 was synthesized by  
105 University Sapienza, Rome IT. For MC2494 synthesis details, see Supplementary notes. EX527 (Alexis) was  
106 dissolved in DMSO (Sigma) and used at  $5 \times 10^{-6}$  M, unless otherwise specified. Staurosporine (Alexis) was  
107 dissolved in DMSO and used at  $2 \times 10^{-6}$  M. Suramin (Bio Mol) was used at  $5 \times 10^{-5}$  M.

108

109 **Antibodies.** H3K9-14ac, H3K9ac, H3K56ac and RIP1 were from Diagenode and BD. H4ac and p53ac were  
110 from Upstate. H3, Acetyl-lysine, H4 H2A.X (phS139), CPS1, MLYCD, SirT1, SirT2, PCAF and  
111 KAT1/HAT1 were from Abcam. ATM (phS1981) and ATR were from R&D. Acetyl-tubulin was from  
112 Sigma. ERK1/2, IAP, FLIP-L, PARP and RIP3 were from Santa-Cruz. Bax, t-Bid, caspase 3, caspase 8,  
113 CYLD, IKK $\gamma$ , FADD, FAS, BCL2 were from Cell Signaling. HAT4 was from myBiosource.

114

115 **Morphological analysis.** For U937, MCF7 and MDA-MB-231 cancer cell lines morphological analysis was  
116 performed, using bright field light microscopy (20X).

117

118 **Reagents.** Z-VAD, Z-IETD, Z-LEHD (R&D) were used at 50  $\mu$ M. N-Acetyl cysteine (NAC) and Nec-1  
119 (Sigma) were used at 50 and 100  $\mu$ M, respectively. 1  $\mu$ g of RIP1, RIP<sup>(K596/599R)</sup> were transfected. H<sub>2</sub>O<sub>2</sub> and  
120 PIETC (Sigma) were used at 1 mM and 10  $\mu$ M, respectively. C646 (Sigma) was used at 50  $\mu$ M.

121

122 **Cell vitality, Cell cycle, differentiation, death and apoptosis.** To study cell vitality, experiments were  
123 performed in triplicate. Cells were diluted 1:1 in Trypan blue (Sigma) and counted. Cell cycle and  
124 differentiation analysis, was performed in triplicate as reported in (17). Apoptosis was measured by caspase  
125 3-7, 8 and 9 (R&D) and quantified by FACS (BD). Apoptosis was measured as pre-G1 DNA fragmentation  
126 or by Annexin V detection as in (17). Apoptosis vs necrosis was measured using apoptosis/necrosis kit as  
127 suggested by the supplier (Enzo life sciences).

128

129 **SirTs, HDACs & PCAF assays.** SirT1, -2 and -3 assays experiments were performed as suggested by the  
130 supplier (BioMol). Moreover, for SirT1, additional assays were performed: i) HRTF assay; ii) BioMol assay  
131 with a different excitation/emission range; iii) SIRTainty assay (Millipore). SirT3 and 6 assays were  
132 performed *in vitro* following the supplier's instructions (ENZO life and Cayman, respectively). To evaluate  
133 the action of MC2494 on SirT4 and 5, we IPed CPS1 and MLYCD (reported as substrates for SirT4 and  
134 SirT5, respectively) and they used in a radiolabelling assay. Finally, both HDAC and PCAF radioactive  
135 assays were performed according to supplier's instructions (Upstate). A detailed description of *in vitro*  
136 assays is reported in Supplementary Material and Methods.

137

138 **Proliferation and migration analysis in real time.** Proliferation and migration analyses were evaluated in  
139 MDA-MB231 cells and performed according to the supplier instruction (xCELLigence, Roche). A detailed  
140 description is in Supplementary Material and Methods.

141

142 **RNA, RT-PCR and Chromatin immunoprecipitation (ChIP).** Total RNA was extracted with Trizol  
143 (Invitrogen) and converted into cDNA using VILO (Invitrogen). RNA extraction and RT-PCR are detailed in



144 the Supplementary Methods. ChIP was carried out as previously reported (18) using H3K9-14ac. More  
145 details are in Supplementary Material and Methods.

146

147 **Protein extraction.** After PBS wash, cell pellets were suspended in lysis buffer (50 mM Tris-HCl pH 7.4,  
148 150 mM NaCl, 1% NP40, 10 mM NaF, 1 mM PMSF and protease inhibitor cocktail). The lysis reaction was  
149 carried out for 15 min at 4°C. Finally, the samples were centrifuged at 13000 rpm for 30 min at 4°C and  
150 protein concentration quantified by Bradford assay (Bio-Rad).

151

152 **Histone extraction.** After stimulation with the indicated compounds cells were collected and washed two  
153 times with PBS. Pellets were resuspended in Triton Extraction Buffer (TEB) (PBS containing 0.5% Triton X  
154 100 (v/v), 2 mM PMSF, 0.02% (w/v) NaN<sub>3</sub>) and the lysis procedure was performed for 10 min at 4°C. The  
155 samples were centrifuged at 2000 rpm for 10 min at 4°C and pellets washed in TEB (half volume). Samples  
156 were then resuspended in 0.2 N HCl and acid histone extraction was carried out overnight at 4°C. The next  
157 day the supernatant was recovered and protein concentration quantified by Bradford assay (Bio-Rad).

158

159 **Nucleus/Cytosol extraction.** Pellet were resuspended in 2-2.5 volumes of NP-40 Buffer (10mM Tris-HCl  
160 pH 7.0, 10mM NaCl, 3mM MgCl<sub>2</sub>, 30mM Sucrose, 0.5 % NP-40) and incubate for 10' on a rotating  
161 platform at 4°C. After centrifugation at 1000 rpm for 10 min at 4°, the supernatant were transfer in a new  
162 tube (cytosolic fraction). Pellet (nuclei) were suspended in 2 mL of NP-40 Buffer and centrifuged at 3000  
163 rpm for 10 min. The supernatant were removed and the pellet of nuclei was washed in Lysis Buffer (20mM  
164 Tris-HCl pH8, 137mM NaCl, 10% glycerol, 1% NP-40, 2mM EDTA) for 10 min in ice. The suspension was  
165 sonicated (4x 30''off/ 30''on high power). Spin out debris 14.000 rpm for 5 min at 4°and the nuclear proteins  
166 were transfer in a new tube.

167

168 **Western Blot.** 50 µg of proteins were loaded on 10-15% polyacrylamide gels. 5-10 µg of histone extract was  
169 loaded on 15% polyacrylamide gel. The nitrocellulose filters were stained with Ponceau red (Sigma) as  
170 additional control for equal loading. The antibody used, are listed in Supplementary Material and Methods.

171

172 **Immunoprecipitation assay.** MDA-MB-231 and HEK293FT cells were lysed in NP-40 (0.5%), Tris-HCl  
173 pH 8.0 (20 mM), NaCl, (150 mM), PMSF (1 mM), 10% glycerol, EDTA (1 mM) and 1X protease inhibitor  
174 mix (Sigma) for 20' on ice. Cell debris was removed and the protein soluble fraction was incubated with  
175 antibody overnight at 4°C. The immune complexes were immunoprecipitated with Sepharose-protein A/G  
176 Plus (Santa-Cruz) or with GFP -TRAP\_A beads (Cromotech) for 2h at 4°C. Proteins were then eluted,  
177 resuspended and analyzed by western blot.

178

179 **CETSA assay.** HEK293FT cells were harvested and washed with PBS after treatment with  
180 MC2494 (50 µM) and an equal amount of DMSO, as control, for 1 h. The respective samples were

181 suspended in PBS (1.5 mL), divided into aliquots (100  $\mu$ l), and heated at different temperatures  
182 (25°-37°-44°-53°-57°) for 3 min by Thermo Mixer (Eppendorf, Milan, Italy), followed by cooling  
183 for 3 min at 4C. After incubation, lysis buffer (100  $\mu$ l) was added to the samples and incubated for  
184 15 min. The samples were then centrifuged at 13,000 rpm for 30 min at 4°C, the supernatant was  
185 removed and protein concentration was determined using a Bradford assay (Bio-Rad). Of the total  
186 protein extract, 20  $\mu$ g was loaded on 10% SDS-PAGE and western blott analysis was performed.  
187 The antibody used were SirT1, SirT2 and SirT3 (Abcam).

188

189 **Transfections.** RIP1-GFP, RIP-GFP<sup>(K596/599R)</sup> were transfected in HEK293FT cells with Lipofectamine 2000  
190 (Invitrogen). TRAIL promoter mutants were used as previously described (17).

191

### 192 **RNA interference**

193 To silence RIP1 and Caspase8 were used specific pre-designed siRNA for RIP1 (SI00288092) and CASP8  
194 (SI02661946) purchased from Qiagen. U937 cells were transfected with Nucleofector™ Technology and  
195 siRNA were used at 1  $\mu$ M. To silence SIRT1 gene expression, HEK293 cells were transfected with a  
196 specific SirT1 siRNA directed against human SirT1 (On-Target plus SMART pool), which was  
197 purchased from Dharmacon, and with a specific pre-designed siRNA for SirT1 purchased from Ambion.  
198 A scrambled siRNA was used as a control. Cells were transfected with the indicated siRNAs at 50 nM of  
199 concentration, using DharmaFECT1 Transfection reagent (Dharmacon).

200

201 **Allograft experiments.** All animal procedures were conducted according to national and international  
202 guidelines. The breast cancer 4T1–Luc model was a gift from Dr. P. Steeg, (NIH, Bethesda, USA). Approval  
203 was obtained from the Institutional Animal Care and Ethical Committee at CEINGE and “Federico II”  
204 University of Naples (Protocol #29, 01/09/2009), and the Italian Ministry of Health, Dipartimento Sanità  
205 Pubblica Veterinaria D.L. 116/92, confirming that all of the experiments conform to the relevant regulatory  
206 standards. A detailed description of procedures is in Supplementary Material and Methods.

207

208 **Cancer prevention & mito-mice.** MC2494 was dissolved in DMSO and diluted 1:5 in vehicle (corn oil).  
209 7,12-dimethylbenz( $\alpha$ )anthracene (DMBA, Sigma) was dissolved in acetone (8 mM). 8 female MITO-Luc  
210 mice (repTOP™ mitoIRE, Italy) (19) 2 months of age were housed in plastic cages, fed *ad libitum* with a  
211 standard diet (4RF21 standard diet, Mucedola, Italy). Room temperature was within 22-25°C and humidity  
212 of 50  $\pm$  10%. Animals were divided into two groups and s.c. treated with 50 mg/kg MC2494 or placebo (corn  
213 oil) every day at 02.00 PM for 9 days. At day 6, mice were subjected to a single s.c. intra-glandular injection  
214 of DMBA (left) or vehicle (right gland); at day 9, after the last *in vivo* imaging acquisition, mice were  
215 sacrificed, mammary glands explanted for *ex vivo* imaging and fixed for analysis. A detailed description is in  
216 Supplementary Material and Methods. Imaging *in vivo* procedure was as in (20,21) and is detailed in  
217 Supplementary Material and Methods.

218

219 **Xenograft experiments and Pulse generator *in vivo*.** All procedures involving animals and their care were  
220 conducted in conformity with institutional guidelines, which are in compliance with national (D.L. No. 116,  
221 G.U., Suppl. 40, Feb. 18, 1992; Circolare No. 8, G.U., July 1994) and international (EEC Council Directive  
222 86/609, O.J. L 358. 1, Dec 12, 1987; Guide for the Care and Use of Laboratory Animals, United States  
223 National Research Council, 1996) laws. A detailed description of procedures and histology,  
224 immunohistochemistry and TUNEL assay *in vivo* are explained in Supplementary Material and Methods.

225 High resolution nanoLC–Tandem Mass Spectrometry Mass spectrometry analysis was performed on a Q  
226 Exactive Orbitrap mass spectrometer equipped with an EASY-Spray nano-electrospray ion source (Thermo  
227 Fisher Scientific, Bremen, Germany) and coupled to a Thermo Scientific Dionex UltiMate 3000RSLC nano  
228 system (Thermo Fisher Scientific). A detailed description and data processing are in Supplementary Material  
229 and Methods.

230

231 **IP-Mass spectrometry.** For mass spectrometry analysis RIP1 was overexpressed using a GFP-tagged vector  
232 and immunoprecipitated with GFP-trap\_A beads. The data dependent mass spectra were acquired with the  
233 LTQ-Orbitrap mass spectrometer (Thermo Scientific). A detail description of these procedures is in  
234 Supplementary Material and Methods.

235

## 236 **Results**

### 237 **RIP1 is highly expressed in cancer cells and interacts with HAT1 and SirT1/2**

238 Programmed necrosis or necroptosis is an alternative form of programmed cell death in which the RIP1-  
239 RIP3 complex displays a functional role. To explore RIP1 function in cancer, RIP1 protein levels were  
240 evaluated in different cancer cells (Fig. 1A), showing a generally high expression of RIP1. Mass  
241 spectrometry analysis performed after RIP1 immunoprecipitation (ProteomeXchange, PRIDE database,  
242 dataset identifier PXD007198), identified a new RIP1-HAT1-SirT1 complex (Fig. 1B). RIP1-HAT1-SirT1  
243 complex was validated by western blot. Both RIP3 (with a weak signal) and HAT4, known interactors of  
244 RIP1 and HAT1 respectively (22-24), were found in the complex (Fig. 1C). The fact that both SirT1 and  
245 HAT1 immunoprecipitations were reciprocally detecting RIP1, strongly corroborated and strengthen the  
246 existence of the RIP1-HAT1-SirT1 single complex (Supplementary Fig. S1). The observation that both  
247 HAT1 and SirT1 (and 2) were detectable within the RIP1-IP, prompted us to investigate whether these  
248 acetyltransferases/deacetylases might regulate RIP1 by (de)acetylation. By probing RIP1  
249 immunoprecipitated cells with anti-acetyl-lysine antibody, we observed the presence of an acetylated form of  
250 RIP1 (Fig. 1D). Given that RIP1 acetylation has been very debated (25) and never proven in living cells, to  
251 investigate the location of RIP1 acetylation sites, high-resolution tandem mass spectrometry was applied. To  
252 this end, peptides resulting after digestion with trypsin were separated and analysed by nano-HPLC coupled  
253 to an Orbitrap Q-Exactive mass spectrometer. Data-dependent HCD spectra were obtained on the five most  
254 intense mass peaks generated in each scan at 17500 resolution. Amino acid sequences of high confidence

255 peptides obtained by high-resolution tandem mass spectrometry are reported in Supplementary Fig. S2; S3;  
256 S4 and Supplementary Table S1. Five acetylated lysine residues were identified (Fig. 1E); of these, K115  
257 was localized within the RIP1 kinase domain, whereas K625, K627, K642, K648 were mapped within the  
258 RIP1 death domain, suggesting a potential role for acetylation in RIP1 kinase and cell death-regulating  
259 functions. Given that RIP1 is localised in the cytoplasm (26), HAT1 and SirT1 location in the different  
260 cellular compartments was studied. Interestingly, while RIP1 confirmed exclusive cytosolic localization,  
261 HAT1 and SirT1 were found in both nuclear and cytosolic compartments, with a higher expression in the  
262 cytosol (Fig. 1F).

### 263 264 **RIP1 acetylation module is enhanced by SirT inhibition at sites K596-K599**

265 To assess RIP1, HAT1 and SirT1/2 relationship, we measured RIP1 acetylation using a newly synthesised  
266 pan-SirT inhibitor, MC2494 (Fig. 2A; Supplementary Table S2 and Supplementary note) an AGK-2-related  
267 molecule (27). This compound displays inhibitory actions against SirT1, SirT2 and SirT3/4/5/6, revealing  
268 unique features when compared to SirT1- and 2-selective inhibitors (27-29) (Fig. 2B). The IC<sub>50</sub> values for  
269 SirT1 and 2 inhibition were 38.5 $\mu$ M and 58.6 $\mu$ M, respectively (Supplementary Fig. S5A). While MC2494-  
270 SirT1 modulation was corroborated on a panel of orthogonal *in vitro* assays (Supplementary Fig. S5B),  
271 MC2494 was inactive against both HATs (PCAF) and HDACs (Supplementary Fig. S5C and D), suggesting  
272 high pan-SirT specificity. Direct binding between Sirtuins and MC2494, was corroborated by CETSA assay  
273 (30) (Supplementary Fig. S5E). Interestingly, while the presence of MC2494 protected SirTs from thermal  
274 degradation, SirT1/2/3 mRNA and protein levels were reduced in three different cancer systems by MC2494,  
275 differently from normal cells (Fig. 2C and D), assuming features of cancer-selectivity. In agreement with the  
276 pan inhibitory action, MC2494-induced levels of p53K382 and tubulin acetylation were highly increased, as  
277 were H3 (K9-14ac and K56ac) and H4 acetylations (Supplementary Fig. S5F). Excitingly, a strong increase  
278 of RIP1 acetylation was observed (Fig. 2E) upon MC2494 stimulation strengthening a possible role of SirTs  
279 in modulating RIP1 (de)acetylation. Mass spectrometry analyses were applied to corroborate this data. Under  
280 MC2494 treatment conditions, no qualitative differences were detected in RIP1 acetylation with the  
281 exception of the di-acetylated peptide 592-603 ([M+2H]<sup>+</sup> at m/z 777.88), containing two additional  
282 acetylation sites (K596-K599), only detected following MC2494 treatment (Fig. 2F). Interestingly, this  
283 region was also identified as the top score deacetylation site (P-Value: 0.015) by the Predict(S) algorithm of  
284 the ASEB web server for lysine acetylation/deacetylation site prediction by selecting the database of 129  
285 known deacetylation sites of SirT1. Finally, MC2494 regulated the newly identified RIP1 interactome,  
286 decreasing SirT1 expression in the complex, thus unbalancing SirT1 in favour of HAT1. Also HAT4 and  
287 RIP3 were still detectable with a slight increase of RIP3 (Fig. 2G). Interestingly when the HAT inhibitor  
288 C646 was used, this drug was able to abrogate RIP1 acetylation, corroborating the involvement of the acetyl  
289 transferases in RIP1 acetylation (Supplementary Fig. S6A). This evidence is also supported by the presence  
290 of PCAF in the complex. (Supplementary Fig. S6B). Moreover, a siRNA approach was performed to  
291 corroborate and strengthen this data. Upon SirT1 silencing, RIP1 acetylation increased, clarifying the SirT1-

292 mediated action mechanism of MC2494. (Fig. 2H). These results indicate that RIP1 acetylation at K596-  
293 K599 is governed by SirT inhibition using this novel pan-SirT inhibitor. To gain more insights into the role  
294 of MC2494 in RIP1 acetylation, immunoprecipitation assay was carried out in cells stimulated with one  
295 inactive derivative of MC2494, MC2582 (Supplementary Table S2). As expected, MC2582 has no effect on  
296 RIP1 acetylation. (Supplementary Fig. S7).

### 297 298 **Pan SirT inhibition induces caspase 8 dependent cancer-selective cell death**

299 To define the potential biomedical effects of pan-SirT inhibition and RIP1 complex acetylation the action of  
300 MC2494 was investigated on both leukaemia and breast (BC) cancer cells. In contrast to EX527 (SirT1i) and  
301 AGK-2 (SirT2i), MC2494 induced strong proliferation arrest (Fig. 3A and Supplementary Fig S8-S9C) and  
302 importantly, did not affect cell cycle or differentiation (Supplementary Fig. S9A and B). When quantified in  
303 real time, MC2494 reduced cell proliferation and migration rate measured by cell index and slope at early  
304 time points (Fig. 3B). These data strongly imply wide-ranging anti-proliferative effects. Given the  
305 hypothesized tumour-selective action, we evaluated the cytotoxic effect of MC2494 by comparing its effect  
306 on a broad panel of cancer cells and normal (or immortalized, non-cancer) cells. Notably, MC2494 induced  
307 cell death in cancer without displaying significant cytotoxicity in normal cells (Fig. 3C). These findings  
308 strongly suggest that cell death induction by MC2494 is tumour-specific. Caspase-3/7, -8, -9 activation (Fig.  
309 3D) and dissipation of mitochondrial membrane potential (MMD) (Fig. 3E) were induced by MC2494 in  
310 cancer cells as was DNA damage measured as increased expression of ATM, ATR and  $\gamma$ H2AX (Fig. 3F).  
311 Both players of the extrinsic and intrinsic apoptotic pathways were modulated (Supplementary Fig. S9D and  
312 E). To gain mechanistic insights the caspase-8 Z-IETD, caspase-9 Z-LEHD and pan-caspase Z-VAD  
313 inhibitors were tested for their ability to block MC2494 action. Only Z-IETD and ZVAD completely blocked  
314 MC2494-induced programmed cell death (PCD), whereas cell death was unaltered in presence of Z-LEHD  
315 suggesting that caspase-9 activation is dispensable (Fig. 3G). Interestingly, an increment of ROS production  
316 occurred upon MC2494 treatment indicating a possible link between caspase activation, ROS production and  
317 RIP1 expression (Fig. 3H) (31). Therefore, we tested the effect of N-acetyl-cysteine (NAC) (32), a known  
318 ROS scavenger. Remarkably, in U937 cells, NAC abolished MC2494-induced PCD demonstrating a causal  
319 relevance for ROS production (Fig. 3H).

### 320 321 **RIP1 and its acetylation causally activate cancer-selective cell death pathways**

322 To gain insights into PCD mechanism(s), we analysed the transcriptome of U937 cells treated with MC2494  
323 in comparison with cells treated with the lead SirT1 inhibitor EX527 (Supplementary Fig. S10A). The 1245  
324 MC2494 specifically modulated probes were characterized for their relative abundance of Gene Ontology  
325 Biological Processes using DAVID (Supplementary Fig. S10B -11). MC2494 deregulated 116 annotated  
326 genes related to PCD (fdr=0,0029) suggesting that this modulation might account for its apoptotic action (or  
327 part of it). Strikingly, among the PCD-related targets, DR5 was selectively up-regulated by MC2494  
328 (Supplementary Fig. S10C,  $p < 0,001$ ), suggesting that its modulation may account for a potential cancer-



329 selective PCD. Corroborating the transcriptome, PCR confirmed DR5 induction and supported TRAIL  
330 mRNA up-regulation by MC2494 already after 24h of induction. Interestingly, H3ac ChIP followed by  
331 qPCR revealed strong acetylation at TRAIL and DR5 promoters after the treatment (Fig. 4A). To elucidate  
332 the acetylation modulation at TRAIL and DR5 promoters, SirT1 ChIP followed by qPCR was performed.  
333 Interestingly, SirT1 occupancy was found at those promoters and was decreased after MC2494 treatment,  
334 suggesting an active role for SirT1 at TRAIL and DR5 promoters (Fig. 4B). We investigated TRAILp by a  
335 deletion mapping approach (Fig. 4C). Whereas HDACi selectively target the proximal GC-box and  
336 complexes binding to it (17), MC2494-dependent TRAIL activation was strongly reduced by mutations of  
337 promoter-distal areas containing the distal GC-box, AP-1 and ISRE. Conversely, mutation of promoter-  
338 proximal GC-box led to over 2.5-fold increase, highlighting a potential repressive role of MC2494 on  
339 chromatin at this region. Thus, MC2494-driven TRAIL activation causally activates the tumour-selective  
340 TRAIL/DR5 pathway. To extend the hypothesis that both caspase-8 and RIP1 causally act during MC2494  
341 PCD, we performed loss-of-function experiments in U937 cells. Upon silencing of either caspase-8 or RIP1,  
342 MC2494-mediated PCD was abolished, suggesting a potentially crucial link between caspase-8 activation  
343 and RIP1 function (33) in promoting PCD by MC2494 (Fig. 4C). In support, a similar PCD suppression was  
344 observed when pharmacologically blocked RIP1 function after the co-administered with its inhibitor  
345 Necrostatine-1 (Nec-1) (34) (Fig. 4D). Since RIP1 regulates different types of cell death and survival, we  
346 aimed to further distinguish between PCD and necrosis. Data with double Annexin V-propidium iodide (PI)  
347 staining strongly indicated that MC2494, like staurosporine, only induced PCD (Fig. 4E). Intriguingly,  
348 expression of the E3 ubiquitin ligases IAPs is fully abrogated (35) (Fig. 4E), whereas the expression of IKK $\gamma$   
349 (NEMO)(36) is induced in absence of a principal deubiquitinating enzyme, CYLD (37,38) (Fig. 4F).  
350 Collectively, the data suggest a scenario in which, following SirT inhibition by MC2494 treatment, a PCD  
351 pathway is activated, with RIP1 and caspase-8 mediating death and having a causal role. Since RIP1 is  
352 acetylated and in presence of MC2494 the new acetylation occurs at site 596-599 in the RIP1 death domain,  
353 we applied a mutational approach. Upon transfection in cancer cells, RIP1-mediated cell death was reduced  
354 of about 40% with the mutant K596-599R, suggesting that these newly acetylated sites may regulate RIP1  
355 apoptotic function (Fig. 4G). To strength this data, we investigated the effect of MC2494 on RIP1<sup>K596-599R</sup>  
356 (Fig. 4H). While the point mutation has no impact on the binding between HAT1 and RIP1, cell death  
357 induction and RIP1 acetylation undergo to a reduction, suggesting the important role of these K residues in  
358 driving anticancer activity of MC2494 (Fig. 4I).

359

### 360 **MC2494 exerts cancer cell-selective action *ex vivo* and *in vivo***

361 For primary cancers, acute leukaemia blasts were treated *ex vivo* with MC2494 showing a strong increment  
362 in pre-G1 phase (Fig. 5A). MC2494-mediated PCD was clearly detectable at 24 and 48 hours in all 9 primary  
363 acute myeloid leukaemia (AML) blasts and one acute lymphoid leukaemia (ALL) blast, underscoring that in  
364 primary cancer, MC2494 induces apoptosis (Fig. 5A and Supplementary Table S3). Pharmacokinetic and *in*  
365 *vitro* half-life studies strengthened a possible use of MC2494 *in vitro* and *in vivo* (Supplementary Fig. 12A-



366 D). *In vivo*, MC2494 strongly reduced tumour growth in allograft models as quantified by direct photon  
367 emission of luciferase-expressing immuno-competent mice (Fig. 5B and Supplementary Table S4).  
368 Moreover, the MDA-MB-231 breast cancer-based xenograft model treated with MC2494 displayed a strong  
369 anticancer effect visible as decreased tumour mass. When MC2494 was inoculated by *in vivo* chemo-  
370 electroporation, the anticancer effect increased, suggesting its potential *in vivo* also in superficial tumours (as  
371 melanoma or other skin tumours in rapid proliferation) (Fig. 5C). Following MC2494, apoptosis (tunnel  
372 assay), histone and non-histone SirT targeting, SirT1, SirT2, RIP1 and KAT1/HAT1 were observed in  
373 tumours (Fig. 5D) extending results obtained in cell lines.

374

### 375 **MC2494 exerts cancer-preventive action *in vivo***

376 It is a widely shared opinion that cancer prevention is a better approach than treatment. A strategy might  
377 include prevention of cancer recurrences and/or action in genetically predisposed patients. Thus, we  
378 evaluated the ability of MC2494 to prevent early proliferation occurring in mammary glands after carcinogen  
379 exposition. Two groups of MITO-Luc reporter mice (19) (on line Methods) were subcutaneously treated  
380 with a daily dose of 50 mg/kg MC2494 or placebo (corn oil) for 9 days (9D); at D6, right and left mammary  
381 glands were exposed to 7,12-Dimethylbenz[a] anthracen (DMBA) or vehicle, respectively. As expected, 3D  
382 after DMBA injection in the left mammary gland, bioluminescent emission was detectable in the mice pre-  
383 treated with placebo (Fig. 6A, placebo). Excitingly, no bioluminescence was detected in the MC2494-pre-  
384 treated animals, suggesting that the compound was able to fully abrogate DMBA-induced malignant  
385 proliferation *in vivo* (Fig. 6A-C). In keeping with these data, Ki-67 proliferation marker was highly  
386 expressed in the mammary glands treated with DMBA (Fig. 6D, lower panel, left), but to a much lower  
387 extent in glands explanted from MC2494-pre-treated mice (Fig. 6D lower panel, right, and Fig. 6E).  
388 Increased acetylation of H3K9 in tissues obtained from MC2494-treated mice confirmed that the MC2494  
389 was inhibiting this and likely other epi-targets (Fig. 6F and Supplementary Fig. S11). These experiments  
390 suggest that MC2494 counteracts hyper-proliferation occurring during the early steps of carcinogenesis,  
391 strongly supporting that MC2494 is not only active against an ‘on-going’ cancer, but also acts in a cancer-  
392 preventive manner *in vivo*.

393

### 394 **Discussion**

395 Our study identifies a new role for Sirtuins and HATs (mainly HAT1) (39) in modulating programmed death  
396 pathways. This occurs via a newly identified RIP1-SirT1/2/HAT1-containing complex and via regulation of  
397 RIP1 acetylation. RIP1 (and its acetylation) might represent a key regulatory restriction point between  
398 survival, stress and death. In full agreement MC2494, a novel pan-SirT inhibitor (SirTi) (40), alters the  
399 HAT1/SirT equilibrium in the RIP1 complex. The fact that our MS approach combined with affinity-based  
400 chromatography enrichment reveals not only the existence of the RIP1/KAT1/SirT axes, but also the  
401 presence of seven RIP1 acetylation sites (the majority of which are in the death domain) adds to a possible  
402 regulatory role for acetylation of RIP1-mediated death. In support, mutation of K596-599 to arginine alters

403 RIP1 apoptotic function, suggesting its complex regulation by post-translational modifications.  
404 The finding that RIP1 is a main player in PCD represents a paradigm shift, identifying (acetylated) RIP1 as  
405 an apoptotic player altered in cancer and a potential target of intervention. Based on our findings, we  
406 hypothesized that Sirtuins play a key role in restricting RIP1-caspase8 apoptosis in cancer. The importance  
407 of caspase8 is demonstrated by its causal role, since pharmacological inhibition and silencing fully block  
408 SirTi-driven death. Pan-SirT inhibition-mediated anticancer activity is also causally linked to ROS and RIP1,  
409 given that treatment with both NAC and Nec-1, and RIP1 silencing, abolish PCD. Whether this action also  
410 accounts for the tumour-specificity of the pan-SirTi remains to be established. Evidence that both TRAIL  
411 and DR5 are up-regulated upon treatment is reminiscent of findings that we (and others) (41) reported for  
412 HDACi (17). The contribution of TRAIL tumour-selective PCD by SirTi is unlikely attributable to HDAC  
413 inhibition as MC2494 does not affect the activity of HDACs. Secondly, cis-acting elements responsible for  
414 MC2494 TRAIL transcriptional activation are distinct from those reported for HDACi (17). While our  
415 findings strongly suggest that anticancer action of pan-SirTi can be linked to RIP1 acetylation and TRAIL-  
416 DR5 axis activation in cancer (42), the possible tumour-selective activity of pan-SirTi via TRAIL is a key  
417 element since normal cells of diverse origin are all insensitive to pan-SirT inhibition. Although the role of  
418 oxidative stress in TRAIL-mediated apoptosis has been reported (43), our data show that impairment of  
419 either caspase-8 or RIP1 fully blocks SirTi action and that RIP1 acetylation mutant is blandly able to  
420 regulate cell death. Possibly, the presence of 7 different RIP1 acetylation sites (only 2 of which, are  
421 modulated in these settings by SirTi) suggests that acetylation might control RIP1 cell death functions in a  
422 very defined manner. These evidences propose the existence of a caspase-8/RIP1ac-dependent death  
423 paradigm of cell death, bound to epigenetic players such as (but not restricted to) Sirtuins and type-B HATs  
424 (HAT1) (44). Interestingly, SirT1 interferes with apoptosis induced by oxidative stress, deacetylating and  
425 activating FOXO1(45) FOXO3a (46), and FOXO4 (47), inducing GADD45 and the mitochondrial  
426 antioxidant manganese superoxide dismutase. Each of these factors might contribute to ROS tolerance by  
427 SirT1 alteration in cancer. Deregulation of ROS production, oxidative stress, and FOXO activity are  
428 essential steps in cancer development and progression. Moreover, SirTi induction of apoptosis is  
429 accompanied by a marked reduction of IAP and FLICE-inhibitory protein (c-FLIP). Interestingly, IAP  
430 reduction (and DR5 activation co-occurrence) was recently reported combining IAP inhibitors with  
431 lexatumumab (48). This combination results in apoptosis and vanguish cancer resistance by caspase-  
432 8/RIP1ac activation. Thus new therapeutic regimens may involve SirTi and remodulation of the RIP1-  
433 containing complexes in cancer bypassing resistance to conventional drugs. Consistently, both xenograft and  
434 allograft *in vivo* cancer models responded to SirT inhibition with arrest of progression and disease regression  
435 along with increase in apoptotic markers, block of proliferation, SirT and HAT1 expression resetting and  
436 acetylation within tumours. *Ex vivo* leukaemia blasts also undergo PCD upon pan-SirT inhibition, suggesting  
437 a broad range of anticancer actions by MC2494. Though a number of anticancer studies involving SirTi *in*  
438 *vivo* have been reported (49,50), to our knowledge, cancer-prevention *in vivo* has never been described. The  
439 ability of pan-SirT inhibition to fully prevent chemically-induced breast carcinogenesis, concomitantly

440 increasing acetylation *in vivo*, *ex vivo* and during quantitative measurements, shows its potential use in  
441 cancer-preventive settings, which has not been demonstrated before *in vivo*. These preventive features might  
442 prove useful in patients who may benefit from a recurrence-preventive approach with low toxicity during  
443 follow-up phases and in cases of established cancer predisposition.

444

#### 445 **Disclosure of Potential Conflict of Interest**

446 The authors declare that they have no conflicts of interest.

447

#### 448 **Authors' Contributions**

449 V.C. performed the main experiments and wrote the manuscript, F.C., A.N., G.C. performed some cell-based  
450 and contributed to the figures assembling. D.R., D.T., A.M. chemistry. R.R., A.P. molecular modelling. P.B.  
451 immunohistochemistry, A.B., E.S., G.C. xenograft data. A.C., R.R., M.R. acetylated sites by MS/MS data;  
452 J.S., H.G.S. MS/MS data RIP1 interactome, P.C., L.M., E.R. MITO-mice data, P.de A., M.Z. allograft data.  
453 L.A. conceived the study and wrote the manuscript.

454

#### 455 **Acknowledgments**

456 Worldwide Cancer Research (AICR) 15-1002; Blueprint 282510; MIUR20152TE5PK; COST  
457 EPICHEMPIO CM1406; EPIGEN-MIUR-CNR; AIRC-17217; PON\_0101227; Programma VALERE:  
458 Vanvitelli per la Ricerca. We thank C. Fisher for linguistic editing, Annamaria Carissimo, Margherita  
459 Mutarelli and Matthias Nees for help in the array analyses and raw data submission.

460

#### 461 **References**

- 462 1. Galluzzi L, Kroemer G. Secondary Necrosis: Accidental No More. *Trends Cancer* 2017;3(1):1-2 doi  
463 10.1016/j.trecan.2016.12.001.
- 464 2. Galluzzi L, Bravo-San Pedro JM, Vitale I, Aaronson SA, Abrams JM, Adam D, *et al.* Essential  
465 versus accessory aspects of cell death: recommendations of the NCCD 2015. *Cell Death Differ*  
466 2015;22(1):58-73 doi 10.1038/cdd.2014.137.
- 467 3. Galluzzi L, Baehrecke EH, Ballabio A, Boya P, Bravo-San Pedro JM, Cecconi F, *et al.* Molecular  
468 definitions of autophagy and related processes. *EMBO J* 2017;36(13):1811-36 doi  
469 10.15252/embj.201796697.
- 470 4. Galluzzi L, Kepp O, Chan FK, Kroemer G. Necroptosis: Mechanisms and Relevance to Disease.  
471 *Annu Rev Pathol* 2017;12:103-30 doi 10.1146/annurev-pathol-052016-100247.
- 472 5. Vandenabeele P, Galluzzi L, Vanden Berghe T, Kroemer G. Molecular mechanisms of necroptosis:  
473 an ordered cellular explosion. *Nat Rev Mol Cell Biol* 2010;11(10):700-14 doi 10.1038/nrm2970.
- 474 6. Galluzzi L, Bravo-San Pedro JM, Kroemer G. Necrosis: Linking the Inflammasome to  
475 Inflammation. *Cell Rep* 2015;11(10):1501-2 doi 10.1016/j.celrep.2015.05.041.
- 476 7. Jouan-Lanhouet S, Riquet F, Duprez L, Vanden Berghe T, Takahashi N, Vandenabeele P.  
477 Necroptosis, *in vivo* detection in experimental disease models. *Semin Cell Dev Biol* 2014;35:2-13  
478 doi 10.1016/j.semcdb.2014.08.010.
- 479 8. Stanger BZ, Leder P, Lee TH, Kim E, Seed B. RIP: a novel protein containing a death domain that  
480 interacts with Fas/APO-1 (CD95) in yeast and causes cell death. *Cell* 1995;81(4):513-23.
- 481 9. Hsu H, Huang J, Shu HB, Baichwal V, Goeddel DV. TNF-dependent recruitment of the protein  
482 kinase RIP to the TNF receptor-1 signaling complex. *Immunity* 1996;4(4):387-96.

- 483 10. Meylan E, Burns K, Hofmann K, Blancheteau V, Martinon F, Kelliher M, *et al.* RIP1 is an essential  
484 mediator of Toll-like receptor 3-induced NF-kappa B activation. *Nat Immunol* 2004;5(5):503-7 doi  
485 10.1038/ni1061.
- 486 11. Sun L, Wang H, Wang Z, He S, Chen S, Liao D, *et al.* Mixed lineage kinase domain-like protein  
487 mediates necrosis signaling downstream of RIP3 kinase. *Cell* 2012;148(1-2):213-27 doi  
488 10.1016/j.cell.2011.11.031.
- 489 12. Micheau O, Tschopp J. Induction of TNF receptor I-mediated apoptosis via two sequential signaling  
490 complexes. *Cell* 2003;114(2):181-90.
- 491 13. Liu X, Shi F, Li Y, Yu X, Peng S, Li W, *et al.* Post-translational modifications as key regulators of  
492 TNF-induced necroptosis. *Cell Death Dis* 2016;7(7):e2293 doi 10.1038/cddis.2016.197.
- 493 14. Festjens N, Vanden Berghe T, Cornelis S, Vandenabeele P. RIP1, a kinase on the crossroads of a  
494 cell's decision to live or die. *Cell Death Differ* 2007;14(3):400-10 doi 10.1038/sj.cdd.4402085.
- 495 15. Liu XY, Lai F, Yan XG, Jiang CC, Guo ST, Wang CY, *et al.* RIP1 Kinase Is an Oncogenic Driver in  
496 Melanoma. *Cancer Res* 2015;75(8):1736-48 doi 10.1158/0008-5472.CAN-14-2199.
- 497 16. Lalaoui N, Brumatti G. Relevance of necroptosis in cancer. *Immunol Cell Biol* 2017;95(2):137-45  
498 doi 10.1038/icb.2016.120.
- 499 17. Nebbioso A, Clarke N, Voltz E, Germain E, Ambrosino C, Bontempo P, *et al.* Tumor-selective  
500 action of HDAC inhibitors involves TRAIL induction in acute myeloid leukemia cells. *Nature*  
501 *medicine* 2005;11(1):77-84 doi 10.1038/nm1161.
- 502 18. Nebbioso A, Pereira R, Khanwalkar H, Matarese F, Garcia-Rodriguez J, Miceli M, *et al.* Death  
503 receptor pathway activation and increase of ROS production by the triple epigenetic inhibitor  
504 UVI5008. *Molecular cancer therapeutics* 2011;10(12):2394-404 doi 10.1158/1535-7163.MCT-11-  
505 0525.
- 506 19. Goeman F, Manni I, Artuso S, Ramachandran B, Toietta G, Bossi G, *et al.* Molecular imaging of  
507 nuclear factor-Y transcriptional activity maps proliferation sites in live animals. *Molecular biology*  
508 *of the cell* 2012;23(8):1467-74 doi 10.1091/mbc.E12-01-0039.
- 509 20. Ciana P, Raviscioni M, Mussi P, Vegeto E, Que I, Parker MG, *et al.* In vivo imaging of  
510 transcriptionally active estrogen receptors. *Nature medicine* 2003;9(1):82-6 doi 10.1038/nm809.
- 511 21. Spano D, Heck C, De Antonellis P, Christofori G, Zollo M. Molecular networks that regulate cancer  
512 metastasis. *Seminars in cancer biology* 2012;22(3):234-49 doi 10.1016/j.semcancer.2012.03.006.
- 513 22. Wapenaar H, Dekker FJ. Histone acetyltransferases: challenges in targeting bi-substrate enzymes.  
514 *Clin Epigenetics* 2016;8:59 doi 10.1186/s13148-016-0225-2.
- 515 23. Christofferson DE, Yuan J. Necroptosis as an alternative form of programmed cell death. *Curr Opin*  
516 *Cell Biol* 2010;22(2):263-8 doi 10.1016/j.ceb.2009.12.003.
- 517 24. Cho YS, Challa S, Moquin D, Genga R, Ray TD, Guildford M, *et al.* Phosphorylation-driven  
518 assembly of the RIP1-RIP3 complex regulates programmed necrosis and virus-induced  
519 inflammation. *Cell* 2009;137(6):1112-23 doi 10.1016/j.cell.2009.05.037.
- 520 25. Narayan N, Lee IH, Borenstein R, Sun J, Wong R, Tong G, *et al.* The NAD-dependent deacetylase  
521 SIRT2 is required for programmed necrosis. *Nature* 2012;492(7428):199-204 doi  
522 10.1038/nature11700.
- 523 26. Wegner KW, Saleh D, Degtarev A. Complex Pathologic Roles of RIPK1 and RIPK3: Moving  
524 Beyond Necroptosis. *Trends Pharmacol Sci* 2017;38(3):202-25 doi 10.1016/j.tips.2016.12.005.
- 525 27. Outeiro TF, Kontopoulos E, Altmann SM, Kufareva I, Strathearn KE, Amore AM, *et al.* Sirtuin 2  
526 inhibitors rescue alpha-synuclein-mediated toxicity in models of Parkinson's disease. *Science*  
527 2007;317(5837):516-9 doi 10.1126/science.1143780.
- 528 28. Trapp J, Meier R, Hongwiset D, Kassack MU, Sippl W, Jung M. Structure-activity studies on  
529 suramin analogues as inhibitors of NAD+-dependent histone deacetylases (sirtuins). *ChemMedChem*  
530 2007;2(10):1419-31 doi 10.1002/cmdc.200700003.
- 531 29. Napper AD, Hixon J, McDonagh T, Keavey K, Pons JF, Barker J, *et al.* Discovery of indoles as  
532 potent and selective inhibitors of the deacetylase SIRT1. *J Med Chem* 2005;48(25):8045-54 doi  
533 10.1021/jm050522v.
- 534 30. Jafari R, Almqvist H, Axelsson H, Ignatushchenko M, Lundback T, Nordlund P, *et al.* The cellular  
535 thermal shift assay for evaluating drug target interactions in cells. *Nat Protoc* 2014;9(9):2100-22 doi  
536 10.1038/nprot.2014.138.
- 537 31. Linkermann A, Green DR. Necroptosis. *N Engl J Med* 2014;370(5):455-65 doi  
538 10.1056/NEJMra1310050.



- 539 32. Sun SY. N-acetylcysteine, reactive oxygen species and beyond. *Cancer Biol Ther* 2010;9(2):109-10.  
540 33. Newton K, Dugger DL, Wickliffe KE, Kapoor N, de Almagro MC, Vucic D, *et al.* Activity of  
541 protein kinase RIPK3 determines whether cells die by necroptosis or apoptosis. *Science*  
542 2014;343(6177):1357-60 doi 10.1126/science.1249361.  
543 34. Degterev A, Hitomi J, Germscheid M, Ch'en IL, Korkina O, Teng X, *et al.* Identification of RIP1  
544 kinase as a specific cellular target of necrostatins. *Nat Chem Biol* 2008;4(5):313-21 doi  
545 10.1038/nchembio.83.  
546 35. Bertrand MJ, Milutinovic S, Dickson KM, Ho WC, Boudreault A, Durkin J, *et al.* cIAP1 and cIAP2  
547 facilitate cancer cell survival by functioning as E3 ligases that promote RIP1 ubiquitination. *Mol*  
548 *Cell* 2008;30(6):689-700 doi 10.1016/j.molcel.2008.05.014.  
549 36. Biton S, Ashkenazi A. NEMO and RIP1 control cell fate in response to extensive DNA damage via  
550 TNF-alpha feedforward signaling. *Cell* 2011;145(1):92-103 doi 10.1016/j.cell.2011.02.023.  
551 37. O'Donnell MA, Legarda-Addison D, Skountzos P, Yeh WC, Ting AT. Ubiquitination of RIP1  
552 regulates an NF-kappaB-independent cell-death switch in TNF signaling. *Curr Biol* 2007;17(5):418-  
553 24 doi 10.1016/j.cub.2007.01.027.  
554 38. O'Donnell MA, Hase H, Legarda D, Ting AT. NEMO inhibits programmed necrosis in an  
555 NFkappaB-independent manner by restraining RIP1. *PLoS One* 2012;7(7):e41238 doi  
556 10.1371/journal.pone.0041238.  
557 39. Parthun MR. Histone acetyltransferase 1: more than just an enzyme? *Biochim Biophys Acta*  
558 2013;1819(3-4):256-63.  
559 40. Mellini P, Valente S, Mai A. Sirtuin modulators: an updated patent review (2012 - 2014). *Expert*  
560 *Opin Ther Pat* 2015;25(1):5-15 doi 10.1517/13543776.2014.982532.  
561 41. Insinga A, Monestiroli S, Ronzoni S, Gelmetti V, Marchesi F, Viale A, *et al.* Inhibitors of histone  
562 deacetylases induce tumor-selective apoptosis through activation of the death receptor pathway.  
563 *Nature medicine* 2005;11(1):71-6 doi 10.1038/nm1160.  
564 42. Kim HB, Kim MJ, Lee SH, Lee JW, Bae JH, Kim DW, *et al.* Amurensin G, a novel SIRT1 inhibitor,  
565 sensitizes TRAIL-resistant human leukemic K562 cells to TRAIL-induced apoptosis. *Biochem*  
566 *Pharmacol* 2012;84(3):402-10 doi 10.1016/j.bcp.2012.03.014.  
567 43. Lee MW, Park SC, Kim JH, Kim IK, Han KS, Kim KY, *et al.* The involvement of oxidative stress in  
568 tumor necrosis factor (TNF)-related apoptosis-inducing ligand (TRAIL)-induced apoptosis in HeLa  
569 cells. *Cancer Lett* 2002;182(1):75-82.  
570 44. Parthun MR. Hat1: the emerging cellular roles of a type B histone acetyltransferase. *Oncogene*  
571 2007;26(37):5319-28 doi 10.1038/sj.onc.1210602.  
572 45. Motta MC, Divecha N, Lemieux M, Kamel C, Chen D, Gu W, *et al.* Mammalian SIRT1 represses  
573 forkhead transcription factors. *Cell* 2004;116(4):551-63.  
574 46. Brunet A, Sweeney LB, Sturgill JF, Chua KF, Greer PL, Lin Y, *et al.* Stress-dependent regulation of  
575 FOXO transcription factors by the SIRT1 deacetylase. *Science* 2004;303(5666):2011-5 doi  
576 10.1126/science.1094637.  
577 47. van der Horst A, Tertoolen LG, de Vries-Smits LM, Frye RA, Medema RH, Burgering BM. FOXO4  
578 is acetylated upon peroxide stress and deacetylated by the longevity protein hSir2(SIRT1). *J Biol*  
579 *Chem* 2004;279(28):28873-9 doi 10.1074/jbc.M401138200.  
580 48. Basit F, Humphreys R, Fulda S. RIP1 protein-dependent assembly of a cytosolic cell death complex  
581 is required for inhibitor of apoptosis (IAP) inhibitor-mediated sensitization to lexatumumab-induced  
582 apoptosis. *J Biol Chem* 2012;287(46):38767-77 doi 10.1074/jbc.M112.398966.  
583 49. Carafa V, Nebbioso A, Altucci L. Sirtuins and disease: the road ahead. *Front Pharmacol* 2012;3:4  
584 doi 10.3389/fphar.2012.00004.  
585 50. Carafa V, Rotili D, Forgione M, Cuomo F, Serrettiello E, Hailu GS, *et al.* Sirtuin functions and  
586 modulation: from chemistry to the clinic. *Clin Epigenetics* 2016;8:61 doi 10.1186/s13148-016-0224-  
587 3.  
588  
589  
590  
591  
592

593 **FIGURE LEGENDS**

594 **Figure 1.** RIP1 expression, interactome, acetylation and location. **A**, RIP1 protein expression in different  
595 cancer cell lines. **B**, Mass spectroscopy analysis of RIP1 interactome performed in HEK293FT RIP1-GFP  
596 cells. **C**, Western blot analysis of RIP1-GFP immunoprecipitated in HEK293FT cells shows the presence of  
597 RIP1, SirT1, KAT1/HAT1, SirT2, HAT4 and RIP3 proteins. **D**, Western blot analysis of RIP1-GFP  
598 immunoprecipitated with GFP Trap\_A beads in HEK293FT cells. *Top panel*: WB with ac-lysines antibody  
599 reveals RIP1 acetylation levels, *Lower panel*: WB for RIP1 and KAT1/HAT1. **E**, Schematic representation  
600 of acetylated lysines and their localization within the RIP1 subdomains. **F**, Nucleo/Cytosol localisation of  
601 RIP1, SirT1 and HAT1 performed in HEK293FT cells.

602 **Figure 2.** The novel pan-SirT inhibitor MC2494 affects RIP1 acetylation. **A**, Structure of MC2494. **B**, *in*  
603 *vitro* inhibition of SirT1/2/3/4/5/6 by MC2494. Enzymatic assays carried out with MC2494 (50  $\mu$ M) and  
604 Suramin (100  $\mu$ M), EX527 (5  $\mu$ M), AGK2 (50  $\mu$ M) were used as controls. **C**, mRNA evaluation of SirT1,  
605 SirT2 and SirT3 in HEK293FT, MDA-MB231 and U937 cancer cells. **D**, mRNA evaluation of SirT1, SirT2  
606 and SirT3 in HACAT “normal” cells. **E**, Western blot analysis of RIP1-GFP immunoprecipitated in  
607 HEK293FT. *Top panel*: WB with ac-lysines antibody reveals a strong increase of RIP1 acetylation levels  
608 after MC2494 treatment, *Lower panel*: WB for RIP1. **F**, Schematic representation of the acetylated lysines  
609 upon MC2494 and their localization within the RIP1 subdomains. Extracted ion chromatogram  
610 corresponding to the monoacetylated RIP1 peptides. **G**, Molecular complex analysis after MC2494  
611 treatment. Western blot analysis of RIP1-GFP immunoprecipitates in HEK293FT cells confirms the presence  
612 of SirT1, HAT1, RIP1, HAT4 and RIP3 proteins. After MC2494 treatment a reduction of SirT1 and a slight  
613 increase of HAT1 is observed. **H**, Evaluation of acetyl RIP1 in SirT1 loss of function condition. Graph  
614 showed the mean of three independent experiments with error bars indicating standard deviation.

615 **Figure 3.** MC2494 affects proliferation and induces caspase8-dependent apoptosis. **A**, Proliferation curve in  
616 U937 cells in presence of the indicated compounds and analysis of cell death as evaluation of preG1 phase.  
617 MC2494 and AGK2 were used at 50  $\mu$ M, EX527 at 5  $\mu$ M. **B**, Left: MDA-MB-231 cell growth following  
618 MC2494, monitored in real time. Right: Migration rate measure as slope (1/h) monitored within the 24 h  
619 from the indicated treatments. MC2494 was used at 50  $\mu$ M. **C**, Induction of preG1 phase upon MC2494  
620 treatment in cancer and normal cell lines. **D**, **E**, FACS analysis of caspase 8, 9 and 3/7 activation and MMD.  
621 The experiments were carry out in U937 cells upon treatment with MC2494 (50  $\mu$ M). **F**, Western blot  
622 analysis of DNA damage evaluation performed in U937 cells upon treatment with MC2494 (50  $\mu$ M). **G**,  
623 apoptosis induced by MC2494 (50  $\mu$ M and 24 h) in U937 cells is selectively blocked by pan- and caspase 8  
624 inhibitors (ZVAD and IETD), but not by caspase 9 (LEHD). **H**, ROS production following MC2494 (50  
625  $\mu$ M), PIETC (10  $\mu$ M) and H<sub>2</sub>O<sub>2</sub> (1 mM) for 24 h, MC2494-mediated apoptosis was blocked by NAC (50  
626  $\mu$ M). Curves and graph presented showed the mean of at least three different experiments with an error bars  
627 indicating standard deviation.

628



629 **Figure 4.** The TRAIL-DR5 axis mediates MC2494 cell death. **A,** TRAIL and DR5 expression upon MC2494  
630 (50  $\mu$ M) for 24-30 h (left), H3K9ac ChIP assay of DR5, TRAIL promoters followed by qPCR (right). **B,**  
631 SirT1 ChIP assay at DR5 and TRAIL promoters followed by qPCR. **C,** Schematic representation of TRAIL  
632 promoter and deletion mapping (*upper*). Transient transfection assay reveals that TRAIL promoter distal  
633 boxes (containing GC-box, AP-1 and ISRE) are essential for activation by MC2494 (*lower*). **D,** siRNA  
634 silencing of caspase 8 or RIP1 and RIP1 pharmacological inhibition with Necrostatine-1 (Nec-1 100  $\mu$ M)  
635 abolishes MC2494 apoptosis in U937 cells. **E,** Apoptosis (left) and necrosis (Annexin/PI) (right) assays  
636 following treatment with MC2494 (50  $\mu$ M) or vehicle for 24 h in U937 cells. **F,** Western blot analysis in  
637 U937 cells shows a reduction of IAP expression, a no-modulation of CYLD and an increment of IKK $\gamma$   
638 protein levels following MC2494 treatment (50  $\mu$ M and 24 h). ERKs are loading controls. **G,** Evaluation of  
639 RIP1-death impairment in HEK293FT cells transfected with RIP1wt or with the RIP<sup>(K596/599R)</sup> mutant. **H,**  
640 Evaluation of cell death induced by MC2494 in HEK293FT cells transfected with RIP1wt or with the  
641 RIP1<sup>(K596/599R)</sup> mutant. **I,** Protein expression evaluation by western blot of acetyl lysine (*upper*) and RIP1  
642 (*lower*) in HEK293FT cells transfected with RIP1wt and RIP<sup>(K596/599R)</sup> mutant. Graph showed the mean of  
643 three independent experiments with error bars indicating standard deviation.

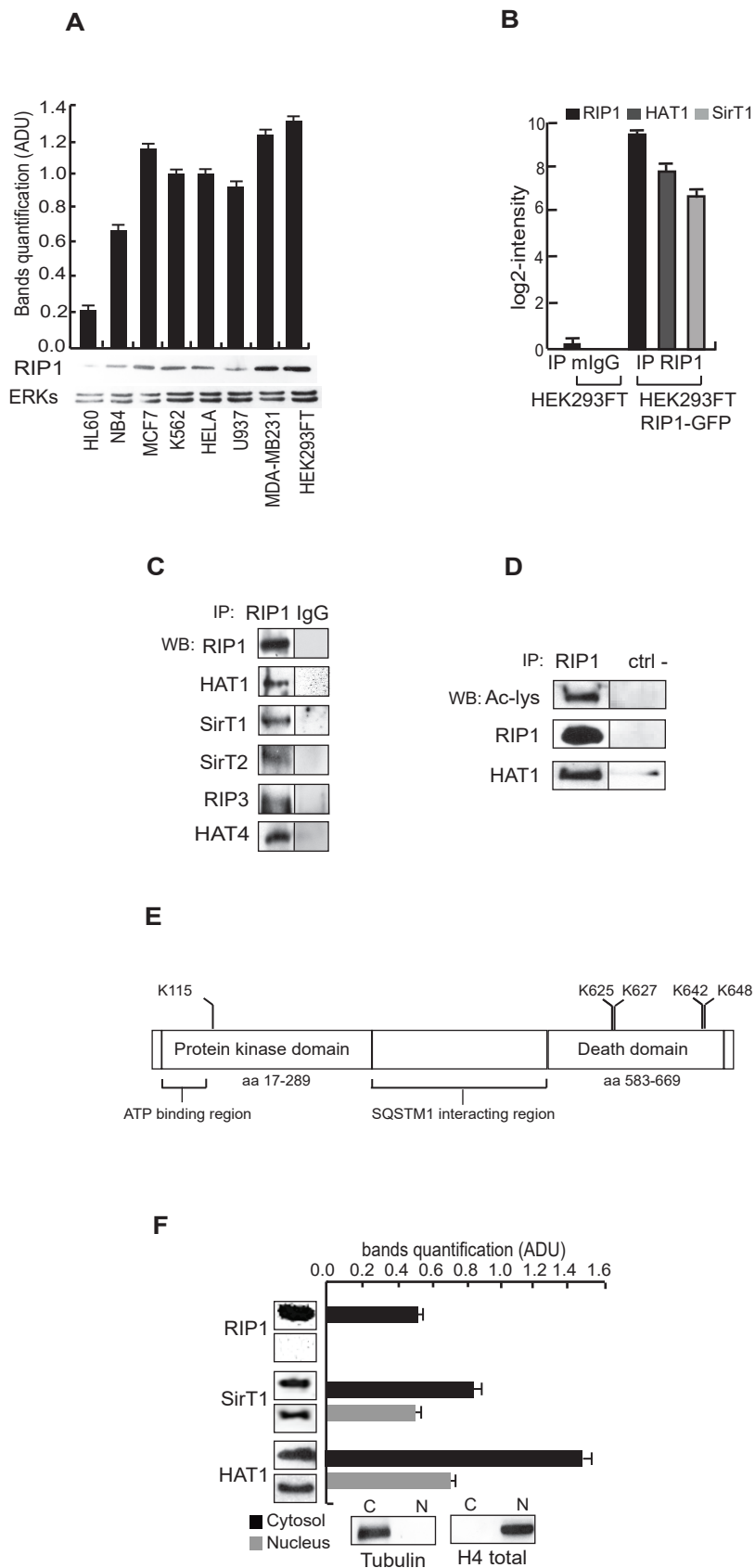
644

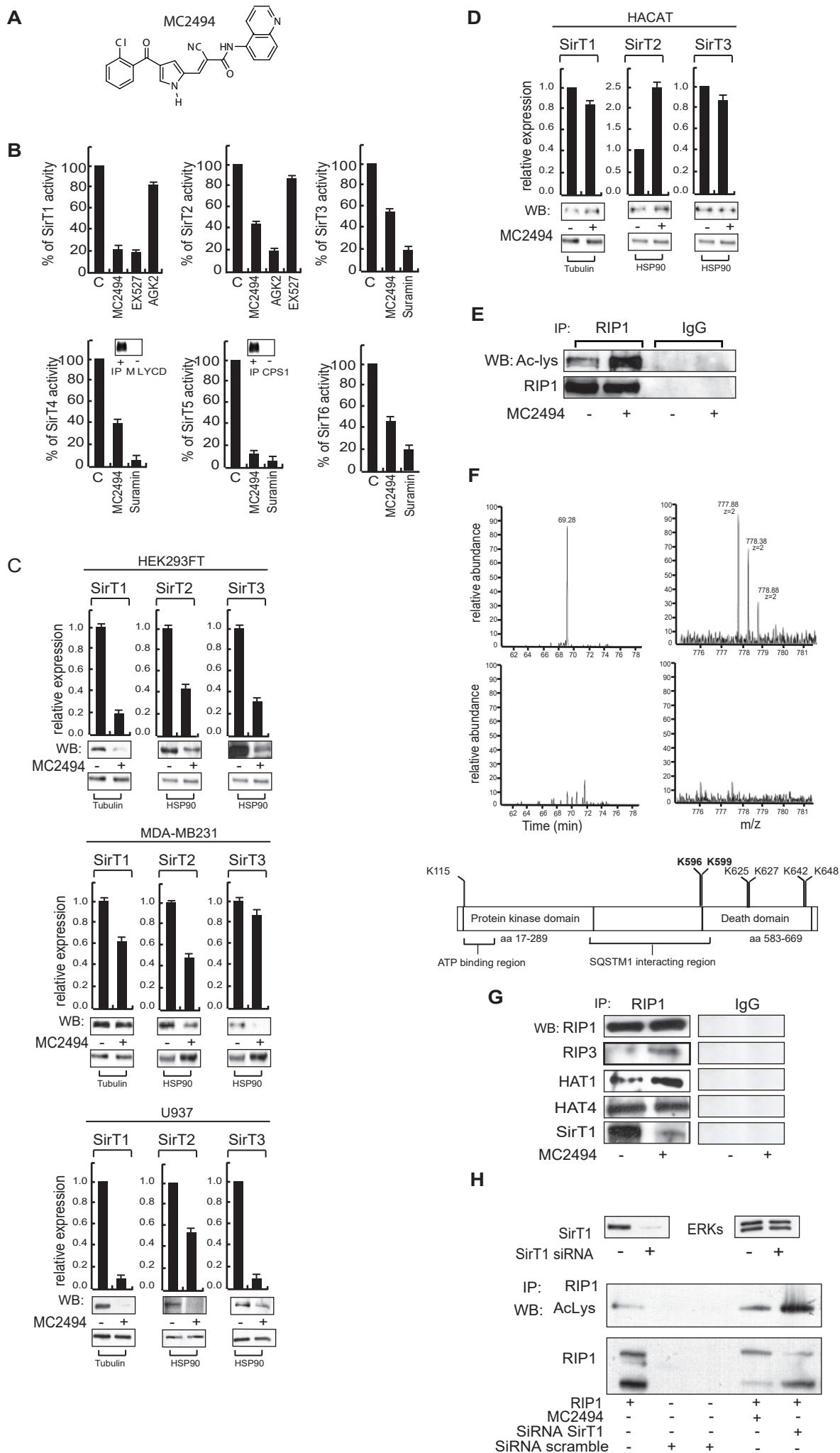
645 **Figure 5.** MC2494 displays broad anticancer action *in vitro*, *ex vivo* and *in vivo*. **A,** Induction of apoptosis by  
646 MC2494 (50  $\mu$ M) for 24 and 48 h in 10 *ex vivo* primary AML and ALL blasts. **B,** Representative images of  
647 two orthotopic allografted mice with 4T1-luc cells into mammary fat pad. Bioluminescence imaging levels  
648 of vehicle- (DMSO) and MC2494-treated mice were acquired at 0 (T0), and after 7 (T7) days of daily  
649 treatment, and quantified as photon/s. See (Supplementary information Table S4) for BLI data in photon/sec.  
650 Results are  $\Sigma \pm$  SEM. from 7 mice each in the vehicle- and MC2494-treated groups. **C,** MC2494 reduces  
651 subcutaneous tumor growth of MDA-MB-231 xenograft using s.c. injection of  $5 \times 10^6$  cells into the left leg of  
652 nude mice by and its combination with electrochemotherapy. *In vivo* growth in volume of tumors induced.  
653 Two controls (vehicle alone and electroporation of vehicle) are reported to exclude possible effects of the  
654 vehicle and electroporation *in vivo*. In the control groups (animals treated with vehicle or electroporation),  
655 tumor volumes strongly increased over a 28-day period whereas MC2494 caused a significant reduction (p  
656 value 0.005 and 0.001, respectively). An even greater growth inhibition was obtained by the combination of  
657 MC2494/electrochemotherapy, (p value < 0.001) compared to both controls. The weight of all mice assigned  
658 to the various groups fell within the same range, providing no immediate evidence for overt toxic effects.  
659 Ki67 and TUNEL scores were performed at the end of treatment. The proliferation index was significantly  
660 lower in tumours of treated mice compared to controls (p=0.002). Apoptotic index was significantly higher  
661 in tumours of MC2494-treated mice (p=0.002). **D,** Immunohistochemical analysis for the apo-index, Ki67,  
662 H3K56ac, ac-tubulin, SirT1, SirT2, RIP1 and KAT1/HAT1 levels in tumours). Curves and graph presented  
663 showed the mean of at least two different experiments with an error bars indicating standard deviation.

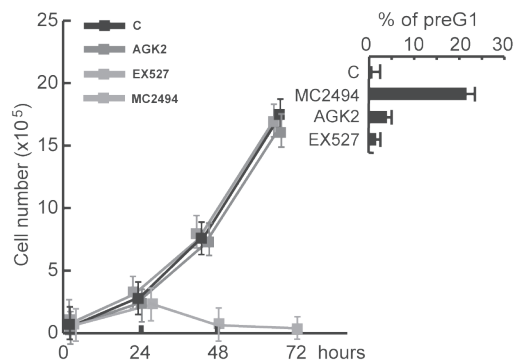
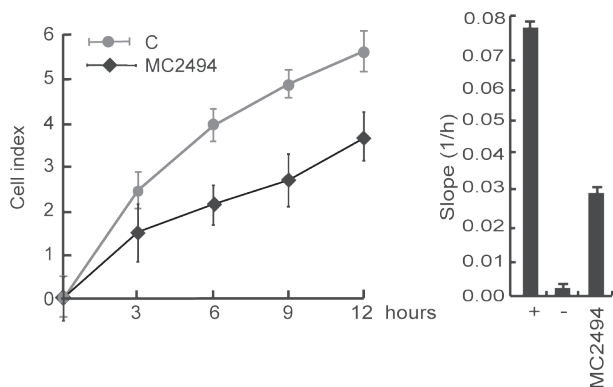
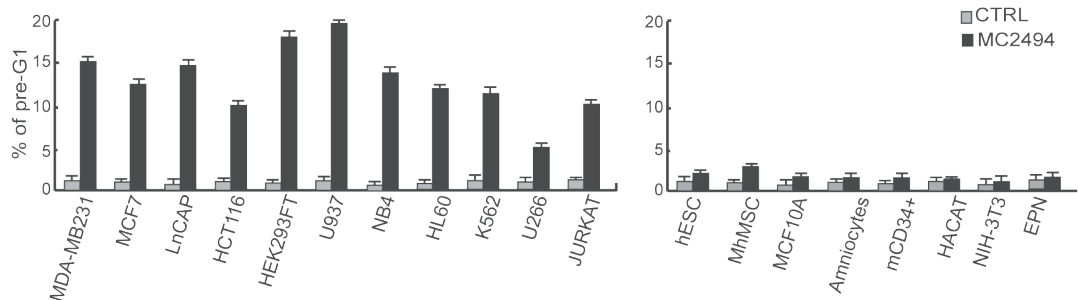
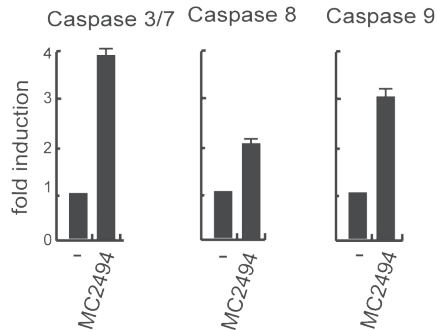
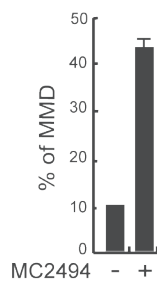
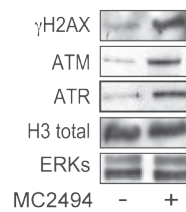
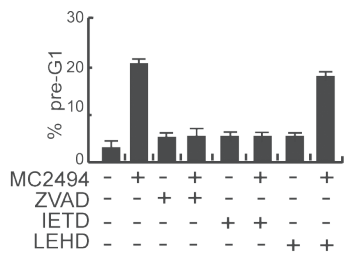
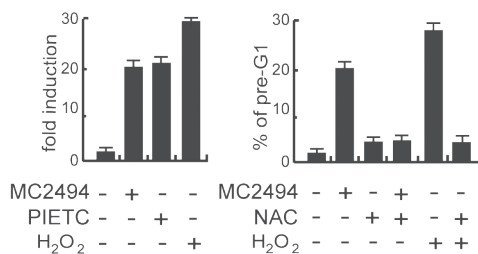
664

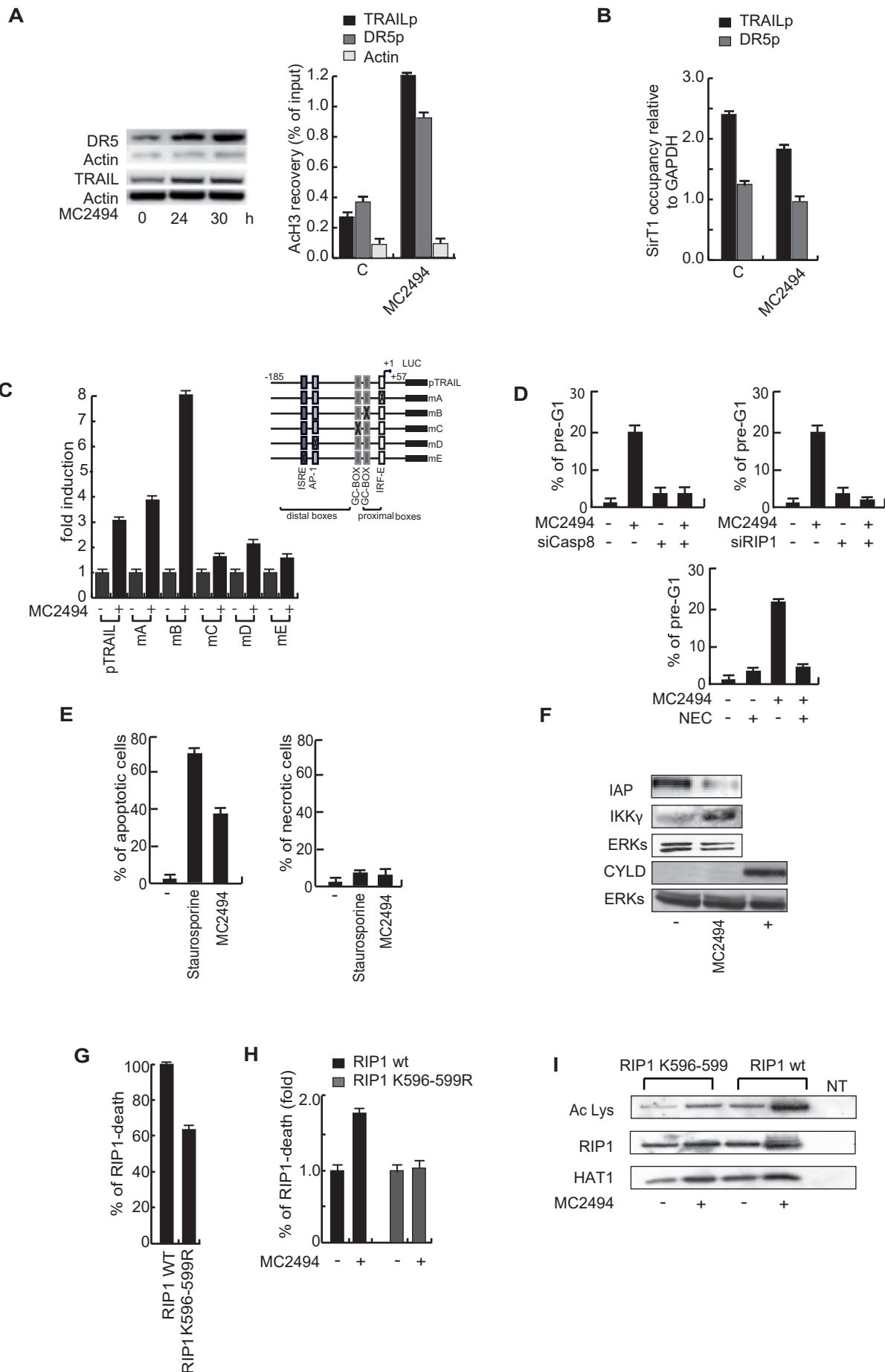
665 **Figure 6.** MC2494 exerts cancer preventive effects *in vivo*. **A**, Optical imaging analysis of bioluminescence  
666 from MITO-Luc reporter mice injected in the mammary fat pad with DMBA (left) or vehicle (right gland);  
667 bioluminescent emission is represented using a pseudo-colour scale. Magnified inserts highlight details of  
668 photon emission from mammary glands. **B**, Quantitation of (A). Bars represent average photon emission  $\pm$   
669 SEM from 4 animals/group measured within the mouse areas shown in the magnified inserts in (A);  
670 bioluminescent emission is completely prevented in MC2494 group as compared to placebo. \*\*\*  $p < 0.001$   
671 DMBA (n=4) vs vehicle-treated (n=4) mammary glands calculated using unpaired t-test. **C**, *Ex vivo* imaging  
672 of mammary glands from 2 representative mice from each group. **D**, Immunohistochemistry of breast slices  
673 obtained from each group stained for Ki67 antibody reveals a marked reduction of cell proliferation in the  
674 DMBA + MC2494 as compared to DMBA. **E**, Quantitation of immunohistochemistry in (d). Bars represent  
675 the average  $\pm$  SEM of the Ki67 index expressed as the ratio between Ki67-positive cells vs total. \*\*\*  $p <$   
676 0.001 DMBA vs vehicle-treated mammary glands calculated using 2-way ANOVA followed by the  
677 Bonferroni *post-hoc* test. **F**, Immunohistochemistry and relative quantization of H3K9 acetylation on breast  
678 slices obtained from each group; increased H3K9ac is visible in MC2494-treated animals corroborating  
679 SirT1/2 inhibition *in vivo*. Graph showed the mean of three independent experiments with error bars  
680 indicating standard deviation.

681

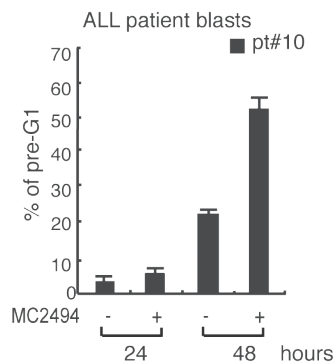
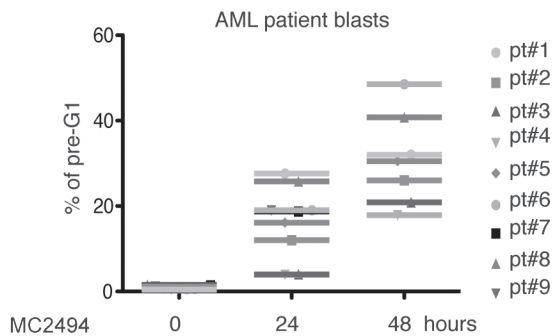
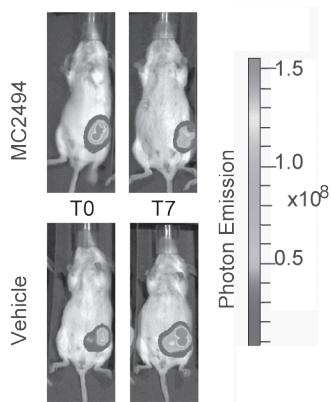
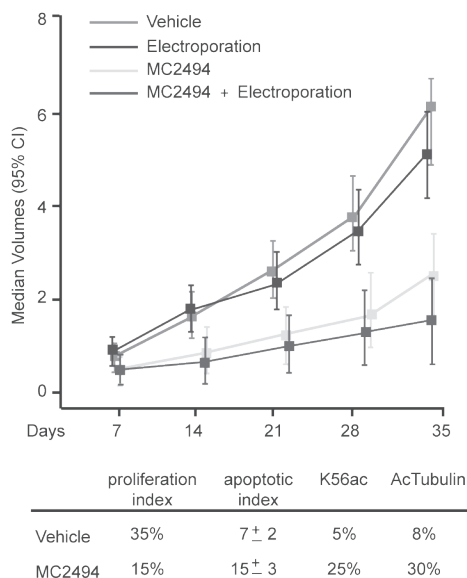
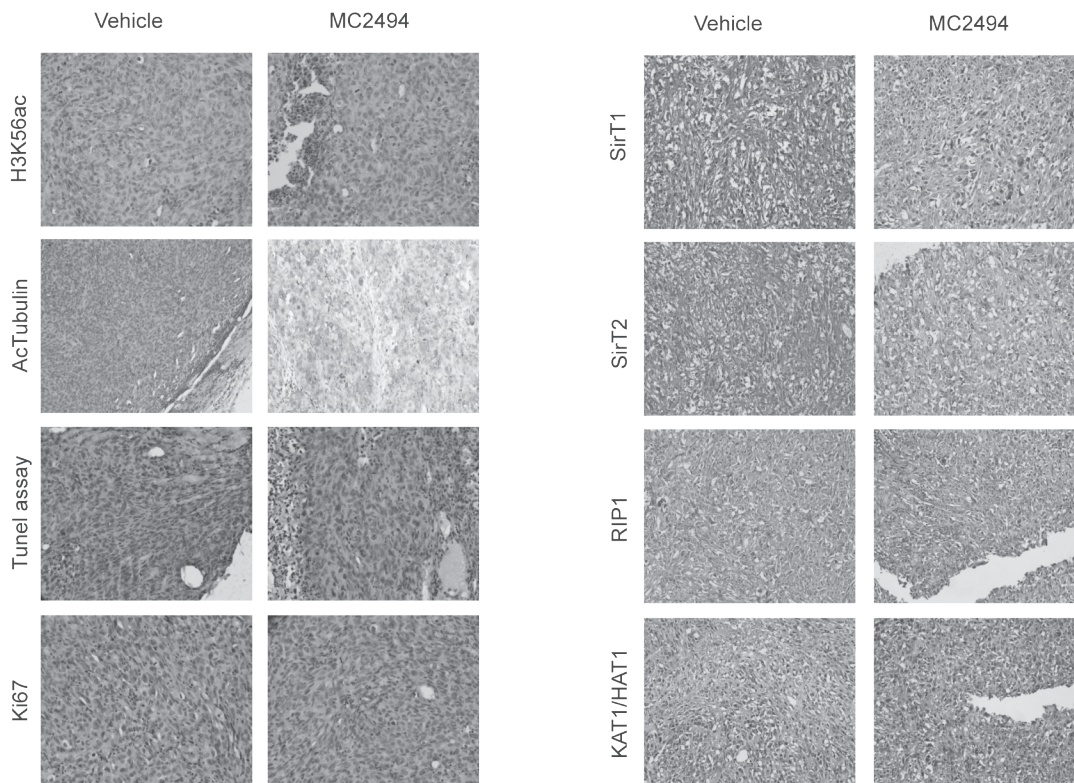


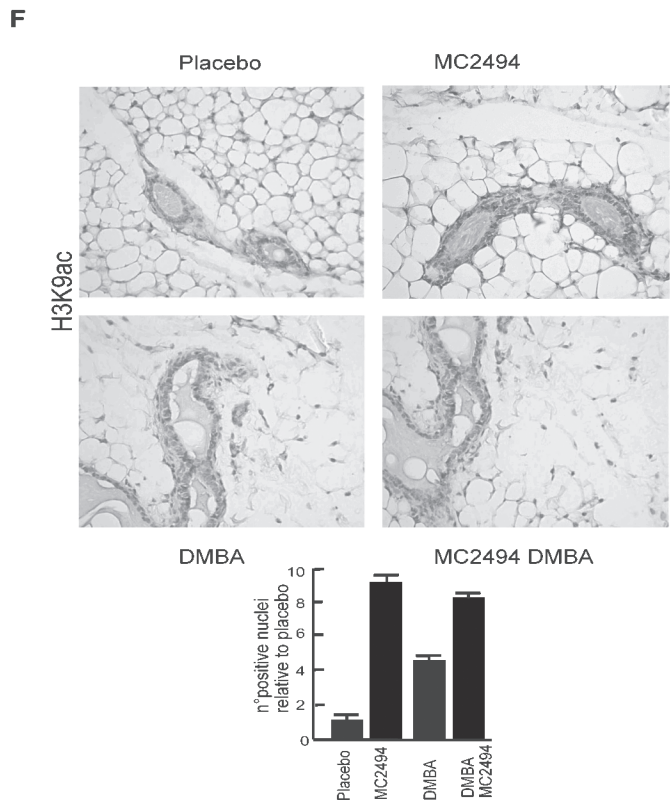
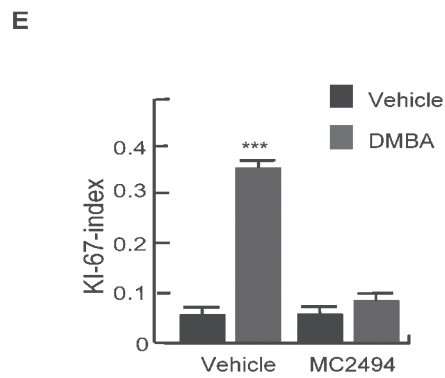
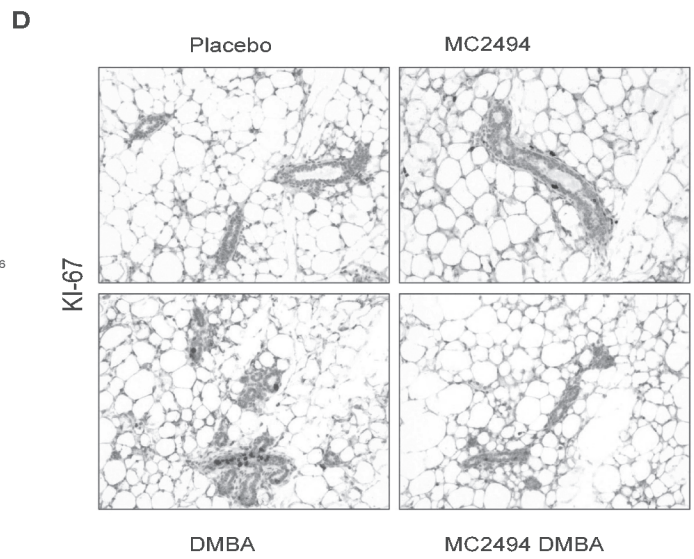
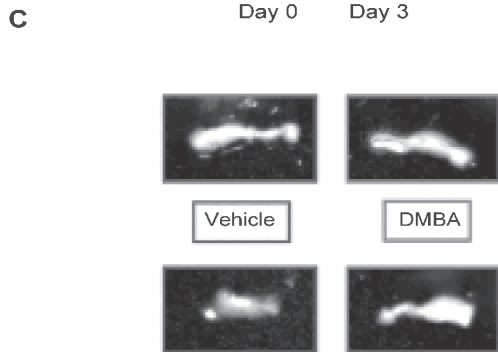
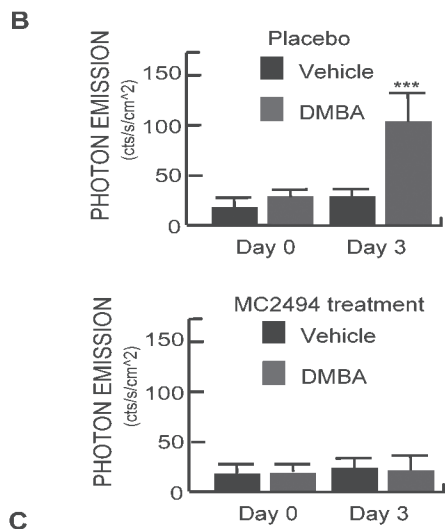
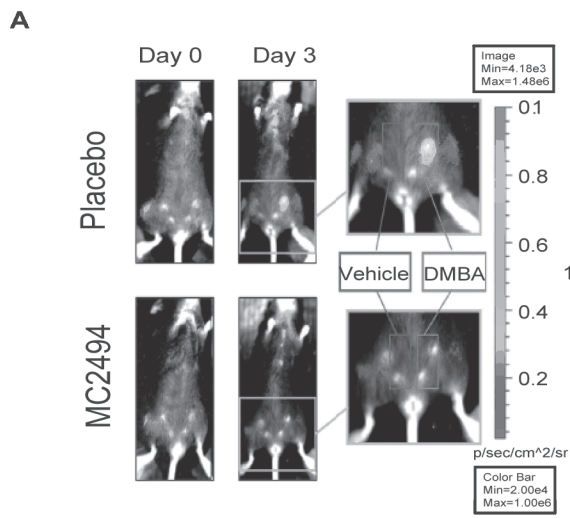


**A****B****C****D****E****F****G****H**





**A****B****C****D**



# Clinical Cancer Research

## RIP1-HAT1-SirT complex identification and targeting in treatment and prevention of cancer

Vincenzo Carafa, Angela Nebbioso, Francesca Cuomo, et al.

*Clin Cancer Res* Published OnlineFirst March 13, 2018.

<b>Updated version</b>	Access the most recent version of this article at: doi: <a href="https://doi.org/10.1158/1078-0432.CCR-17-3081">10.1158/1078-0432.CCR-17-3081</a>
<b>Supplementary Material</b>	Access the most recent supplemental material at: <a href="http://clincancerres.aacrjournals.org/content/suppl/2018/03/13/1078-0432.CCR-17-3081.DC1">http://clincancerres.aacrjournals.org/content/suppl/2018/03/13/1078-0432.CCR-17-3081.DC1</a>
<b>Author Manuscript</b>	Author manuscripts have been peer reviewed and accepted for publication but have not yet been edited.

<b>E-mail alerts</b>	<a href="#">Sign up to receive free email-alerts</a> related to this article or journal.
<b>Reprints and Subscriptions</b>	To order reprints of this article or to subscribe to the journal, contact the AACR Publications Department at <a href="mailto:pubs@aacr.org">pubs@aacr.org</a> .
<b>Permissions</b>	To request permission to re-use all or part of this article, use this link <a href="http://clincancerres.aacrjournals.org/content/early/2018/03/16/1078-0432.CCR-17-3081">http://clincancerres.aacrjournals.org/content/early/2018/03/16/1078-0432.CCR-17-3081</a> . Click on "Request Permissions" which will take you to the Copyright Clearance Center's (CCC) Rightslink site.